J|A|C|S ARTICLES

Published on Web 07/08/2009

Defining Active Catalyst Structure and Reaction Pathways from ab Initio Molecular Dynamics and Operando XAFS: Dehydrogenation of Dimethylaminoborane by Rhodium Clusters

Roger Rousseau,*,† Gregory K. Schenter,† John L. Fulton,† John C. Linehan,† Mark H. Engelhard,‡ and Thomas Autrey†

Fundamental & Computer Sciences Directorate, and W. R. Wiley Environmental Molecular Sciences Laboratory (EMSL) Science Division, Pacific Northwest National Laboratory, Richland, Washington 99352

Received February 25, 2009; E-mail: roger.rousseau@pnl.gov

Abstract: We present the results of a detailed operando XAFS and density functional theory (DFT)-based ab initio molecular dynamics (AIMD) investigation of a proposed mechanism of the dehydrogenation of dimethylaminoborane (DMAB) by a homogeneous Rh_4 cluster catalyst. Our AIMD simulations reveal that previously proposed Rh structures, based on XAFS measurements, are highly fluxional, exhibiting both metal cluster and ligand isomerizations and dissociation that can only be accounted for by examining a finite temperature ensemble. It is found that a fluxional species $Rh_4(H_2BNMe_2)_8^{2+}$ is fully compatible with operando XAFS measurements, suggesting that this species may be the observed catalyst resting state. On the basis of this assignment, we propose a mechanism for catalytic DMAB dehydrogenation that exhibits an energy barrier of approximately 28 kcal/mol.

1. Introduction

Catalysis is ubiquitous in nature and industrial chemical processes. The judicious selection of a catalyst provides the ability to enhance reaction rates and to control chemical reaction pathways. The identification of the active catalytic species along with a characterization of the catalytic reaction pathways is an ongoing challenge in both experimental and computational chemistry.[1] The development of this fundamental insight is critical to help guide development of catalyst materials which are specifically designed for a given outcome. Often the researcher is left to characterize the catalyst resting state ex situ and then use chemical intuition to hypothesize potential reaction pathways. Spectroscopic methods that can be used to identify and follow the fate of the key intermediates formed in a chemical reaction, including catalyst structures, are beneficial to help elucidate mechanistic reaction pathways. However, characterization even under operando conditions is often not definitive enough to provide sufficient atomic level detail to hypothesize a mechanism. As such, first principles electronic structure-based simulations can provide an essential complement to experimental studies by providing detailed atomistic models and spectroscopic characterization that may in turn be used as a basis on which to examine reactivity.

Our research is aimed at designing a catalyst for release of H_2 from aminoboranes. On-board hydrogen storage has been described as a technological bottleneck for transition to a hydrogen-based fuel economy.[2] One particular class of compounds, amine boranes and ammonia borane in particular, have recently received a great deal of attention given the high gravimetric and volumetric density of hydrogen and the promise to meet many of the technical benchmarks required of solid-state hydrogen storage materials for fuel cell (FC)-powered vehicles.[3,4] The thermal decomposition of ammonia borane to yield hydrogen occurs by an apparent second-order kinetic process in solution[5] while the thermal decomposition in the solid state appears to follow a nucleation and growth kinetic process.[6] The high hydrogen content in amine boranes has led to a great interest in catalysis[7] and other approaches[8−10] that will enhance hydrogen release from amine boranes at lower temperatures. It is notable that theory and modeling have been insightful to help elucidate the catalytic reaction pathways leading to hydrogen release from ammonia borane[11] and the reactivity and stability of the associated products.[12]

We have recently shown that operando X-ray absorption fine structure (XAFS) spectroscopy, as applied to reacting systems,

† Fundamental & Computer Sciences Directorate.

‡ W. R. Wiley Environmental Molecular Sciences Laboratory (EMSL) Science Division.

(1) Bell, A. T.; Gates, B. C.; Ray, D. R. Basic Research Needs: Catalysis for Energy. A report from the US Department of Energy Basic Energy Sciences Workshop, 2007. www.sc.doe.gov/bes/reports/list.html.

(2) Crabtree, G. W.; Dresselhaus, M. S.; Buchanan, M. V. *Phys. Today* **2004**, 39.

(3) Hamilton, C. W.; Baker, R. T.; Staubitz, A.; Manners, I. *Chem. Soc. Rev.* **2009**, *38*, 279. (b) Peng, B.; Chen, J. *Energy Environ. Sci.* **2008**, *1*, 479. (c) Marder, T. B. *Angew. Chem., Int. Ed.* **2007**, *46*, 8116.

(4) (a) Baumann, J.; Baitalow, E.; Wolf, G. *Thermochim. Acta* **2005**, *430*, 9. (b) Baitalow, F.; Baumann, J.; Wolf, G.; Jaenicke-Rossler, K.; Leitner, G. *Thermochim. Acta* **2002**, *391*, 159. (c) Wolf, G.; Baumann, J.; Baitalow, F.; Hoffmann, F. P. *Thermochim. Acta* **2000**, *343*, 19.

(5) Shaw, W. J.; Linehan, J. C.; Szymczak, N. K.; Heldebrant, D. J.; Yonker, C.; Camaioni, D. M.; Baker, R. T.; Autrey, T. *Angew. Chem., Int. Ed.* **2008**, *47*, 7493.

(6) Stowe, A. C.; Shaw, W. J.; Linehan, J. C.; Schmid, B.; Autrey, T. *Phys. Chem. Chem. Phys.* **2007**, *15*, 1831.

10.1021/ja901480u CCC: $40.75

Scheme 1. Proposed Rh_4 Catalyst Resting States[a]

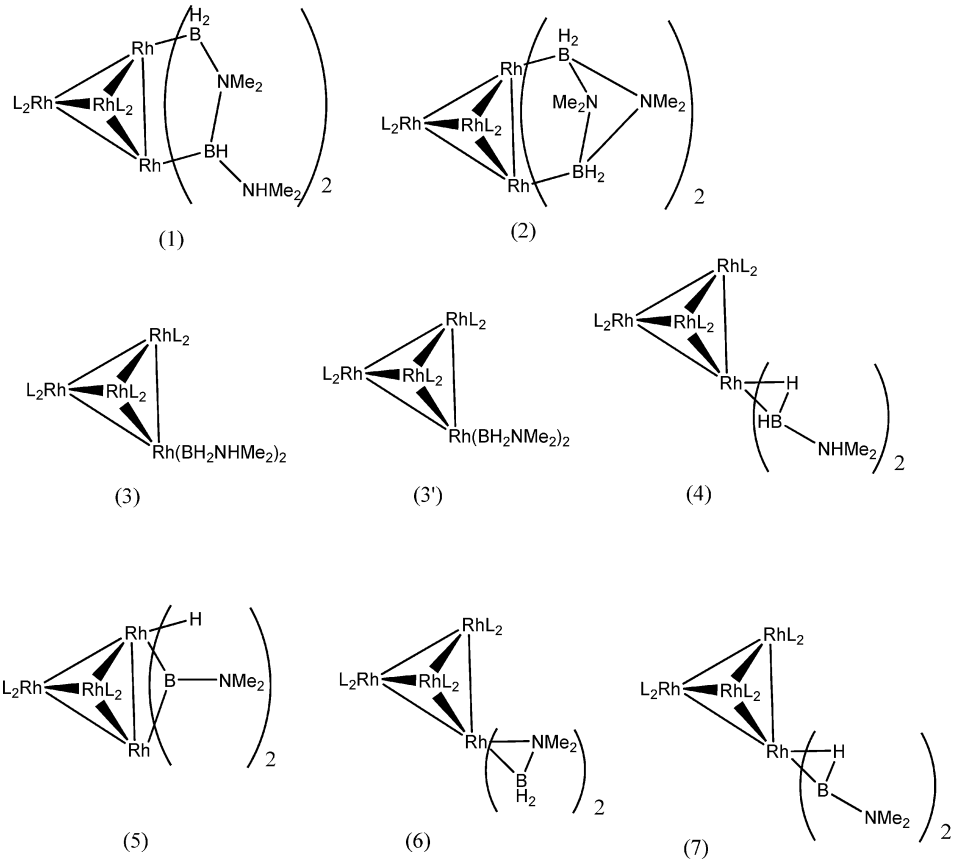

[a] Only a single ligand L is shown explicitly for clarity reasons with all other ligands assumed to be identical. The stick structures, which normally denote bonds between the rhodium and boron atoms, are in these structures used to denote the close proximity of the rhodium and the boron atoms as determined by XAFS. These atoms may indeed be held together by a direct Rh−B bond or by bridging hydrogens, or both vida infra.

can be used to identify the dominant organometallic species formed during the catalyzed release of hydrogen from amine boranes.[7b,13] When coupled with ^{11}B nuclear magnetic resonance (NMR), we were able to follow the decrease in starting material, the increase in boron-containing products, and the correlated transformation of the corresponding rhodium-containing catalytic species. These results lead us to propose a tetrahedral cluster of four rhodium atoms stabilized by the presence of multiple boron hydride donor ligands for the resting state of the catalyst. Upon the basis of the parameters obtained from modeling the XAFS spectra collected during the catalytic reaction, using the ab initio-based FEFF8 software,[14] we proposed five possible candidate structures (**1**−**5** in Scheme 1) for this state. Further consideration has led us to propose three additional species including a variant on structure (**3**) where the amine is deprotonated (denoted **3′**), as well as structures (**6** and **7**) that are consistent with the constraints of the FEFF8 modeling analysis. Note, each species is composed of a cluster of four rhodium atoms in a tetrahedral arrangement with two boron atoms in close proximity to each rhodium. Each boron is bound to a dimethylamine group while these borane amine

(7) (a) Jaska, C. A.; Temple, K.; Lough, A. J.; Manners, I. *J. Am. Chem. Soc.* **2003**, *125*, 9424. (b) Chen, Y. S.; Fulton, J. L.; Linehan, J. C.; Autrey, T. *J. Am. Chem. Soc.* **2005**, *127*, 3254. (c) Clark, T. J.; Russell, C. A.; Manners, I. *J. Am. Chem. Soc.* **2006**, *128*, 9582. (d) Denney, M. C.; Pons, V.; Hebden, T. J.; Heinekey, D. M.; Goldberg, K. I. *J. Am. Chem. Soc.* **2006**, *128*, 12048. (e) Keaton, R. J.; Blacquiere, J. M.; Baker, R. T. *J. Am. Chem. Soc.* **2007**, *129*, 1844. (f) Pons, V.; Baker, R. T.; Szymczak, N. K.; Heldebrant, D. J.; Linehan, J. C.; Matus, M. H.; Grant, D. J.; Dixon, D. A. *Chem. Commun.* **2008**, *48*, 6597. (g) Blaquiere, N.; Diallo-Garcia, S.; Gorelsky, S. I.; Black, D. A.; Fagnou, K. *J. Am. Chem. Soc.* **2008**, *130*, 14034.

(8) (a) Gutowska, A.; Li, L.; Shin, Y.; Wang, C. M.; Li, X. S.; Linehan, J. C.; Smith, R. S.; Kay, B. D.; Schmid, B.; Shaw, W. J.; Gutowski, M.; Autrey, T. *Angew. Chem., Int. Ed.* **2005**, *44*, 3578. (b) Heldebrant, D. J.; Karkamkar, A.; Hess, N. J.; Bowden, M.; Rassat, S.; Zheng, F.; Rappe, K.; Autrey, T. *Chem. Mater.* **2008**, *20*, 5332. (c) Sepehri, S.; Feaver, A.; Shaw, W. J.; Howard, C. J.; Zhang, Q.; Autrey, T. *J. Phys. Chem. B* **2007**, *111*, 14285. (d) Neiner, D.; Karkamkar, A.; Linehan, J. C.; Arey, B.; Autrey, T.; Kauzlarich, S. M. *J. Phys. Chem. C* **2009**, *113*, 1098.

(9) Bluhm, M. E.; Bradley, M. G.; Butterick, R., III; Kusari, U.; Sneddon, L. G. *J. Am. Chem. Soc.* **2006**, *128*, 7748.

(10) Xiong, Z.; Yong, C. K.; Wu, G.; Chen, P.; Shaw, W.; Karkamkar, A.; Autrey, T. *Nat. Mater.* **2008**, *138*, 7. (b) Kanh, X.; Fang, Z.; Kong, L.; Cheng, H.; Yao, X.; Lu, G.; Wang, P. *Adv. Mater.* **2008**, *20*, 2756. (c) Wu, H.; Zhou, W.; Yildirim, T. *J. Am. Chem. Soc.* **2008**, *130*, 14834. (d) Diyabalanage, H. V. K.; Shrestha, R. P.; Semelsberger, T. A.; Scott, B. L.; Bowden, M. E.; Davis, B. L.; Burrell, A. K. *Angew. Chem., Int. Ed.* **2007**, *46*, 8995.

(11) (a) Yang, X.; Hall, M. B. *J. Am. Chem. Soc.* **2008**, *130*, 1798. (b) Paul, A.; Musgrave, C. B. *Angew Chem., Int. Ed.* **2007**, *46*, 8153. (c) Zimmerman, P. M.; Paul, A.; Zhang, Z.; Musgrave, C. B. *Inorg. Chem.* **2009**, *28*, 1069. (d) Blaquiere, N.; Diallo-Garcia, S.; Gorelshy, S. I.; Black, D. A.; Fagnou, K. *J. Am. Chem. Soc.* **2008**, *130*, 14034. (e) Luo, Y.; Ohno, K. *Organometallics* **2007**, *26*, 3597.

(12) (a) Sun, C.-H.; Yao, X.-D.; Du, A.-J.; Li, L.; Smith, S.; Lu, G.-Q. *Phys. Chem. Chem. Phys.* **2008**, *10*, 6104. (b) Gilbert, T. M. *Organometallics* **1998**, *17*, 5513. (c) Li, J.; Kathmann, S.; Schenter, G. K.; Gutowshi, M. *J. Phys. Chem. C* **2007**, *111*, 3294. (d) Nutt, R. M.; Mckee, M. L. *Inorg. Chem.* **2007**, *46*, 7633. (e) Caetano, M. R.; Gerbrand, C. *J. Chem. Phys.* **2007**, *126*, 184703.

(13) Fulton, J. L.; Linehan, J. C.; Autrey, T.; Balasubramanian, M.; Chen, Y. S.; Szymczak, N. K. *J. Am. Chem. Soc.* **2007**, *129*, 11936.

(14) http://leonardo.phys.washington.edu/feff/welcome.html.

ligands attached to the rhodium cluster differ in their connectivity. Recently, a single crystal mono-Rh complex with a dimethylaminoborane ligand was reported[15] where the Rh−ligand interaction is similar to that proposed in structures (**3** and **3′**) which further strengthens the conviction that XAFS studies can provide meaningful structural information in solution phase catalysts. However, two significant structural variables remain undetermined: the net charge on the cluster which effectively determines the Rh oxidation state and number of electrons in the Rh−Rh bonds within the cluster, and the number (if any) of hydride atoms which may be attached to the Rh_4 cluster in addition to the borane ligands. Furthermore, ^{1}H NMR was inconclusive toward observation of any H present on the Rh_4 cluster, i.e., no resonance was observed where metal hydrides are expected, which may be due either to their absence or that the H attached to the cluster is highly mobile on the NMR time scale. Thus, although we were able to identify the presence of a molecular-based rhodium cluster species and general structural features of ligands, we were unable to provide sufficiently detailed information so that the mechanistic details of the dehydrogentation reaction could be inferred.

In the current work we significantly refine our knowledge of the structure of the catalyst resting state by mass spectrometry (MS) and X-ray photoelectron spectroscopy (XPS) that suggest the Rh atoms are in a low oxidation state. With these additional insights we use ab initio molecular dynamics (AIMD)[16] techniques which include finite temperature effects to determine the relative stability of a series of neutral and dicationic rhodium tetrahedral clusters with variable amounts of hydrogen. Using this approach we identify the lowest energy structures that are stable over the course of the MD simulation. We then calculate the XAFS spectra of these structures. We find only one structure that uniquely matches the observed experimental XAFS spectrum. Given a unique solution for the structure, we then further use simulation to test the energetics of a proposed catalytic reaction pathway for dehydrogenation of BH_3NMe_2H (DMAB) by a tetrahedral rhodium cluster.

2. Methods

2.1. Theoretical Simulations. The molecular simulation calculations were carried out using classical molecular dynamics sampling employing density functional theory (DFT) with a gradient corrected functional for exchange and correlation[17] as implemented in the CP2K package.[18] Core electrons are modeled as norm-conserving pseudopotentials and the wave functions expanded in a double-Zeta Gaussian basis set with a planewave auxiliary basis of 200 Ry energy cutoff. We employ periodic boundary conditions in an 18 Å cubic box which provides at least 5 Å separation between the molecules and the closest contact with its nearest neighbor image. For positively charged species, a uniform negative charge background is added leading to a net neutral charge on the simulation cell. Molecular dynamics (MD) simulations are performed in the NVT ensemble using massive Nose−Hoover thermostat chains to maintain a well thermalized sample at 300 K. Once plausible structures for reactant and product states were identified, reaction path analysis was performed using the climbing image nudged-elastic-band method (CI-NEB)[19] employing 8−10 replicas. All simulations are performed without explicit solvent as the XAFS spectra of ref 13 were found to be identical in both THF and toluene indicating minimal solvation effects. This approximation allows us to focus our efforts on the proposed resting state without the additional complexity of modeling the van der Waals interactions (not well reproduced within DFT) between the Rh cluster complex and the solvent.

During the course of our MD simulation effort, over 900 000 DFT cluster configurations were sampled. All MD trajectories were started from partially optimized molecular geometries, based on the structures shown in Scheme 1 with various additional H atoms added to the Rh_4 cluster core. Each structure was equilibrated for a time, Δt_{eq}, which varied from species to species and depended on how long it took to reach the nearest low energy plateau on the potential energy surface as determined from potential energy fluctuations. At this point equilibrated statistics were collected for a time, Δt, over which relative energetics and structural features were evaluated, see Table 1. To address the issue of total charge on the cluster, we have performed MD simulations on neutral, 2+, 4+ charged clusters. After equilibration, an expectation value of the potential energy, $\langle U \rangle$ is obtained for each isomer. This quantity reflects finite temperature (including vibrations) effects as relevant configurations are sampled. Given the observed large fluxional behavior (see below for further discussion), this measure provides a better estimate of the average potential energy of the system than a single ($T = 0$ K) configuration with a harmonic vibrational energy correction. On the other hand, tabulation of $\langle \Delta U \rangle$ is subject to error

Table 1. Relative Energies of Isomers from Scheme 1 at 300 K[a]

species	N_H	x	y	Δt_{eq}(ps)	Δt (ps)	$\Delta U_{x,y}$ (kcal/mol)
			Neutral Species			
1	0	0	0	2.5	1.5	109
1	2	0	1	2.3	1.2	96
1	3	0	2	2.5	1.0	105
2	0	0	0	2.0	1.6	41
2	2	0	1	1.2	1.1	62
2	4	0	2	2.0	1.4	50
3	0	0	4	5.3	2.4	82
3	2	0	5	2.5	2.1	77
3	4	0	6	3.0	1.3	49
3′	0	0	0	6.2	10	47
3′	2	0	1	2.5	17	0
3′	4	0	2	2.0	5.0	25
3′	6	0	3	2.0	1.7	15
3′	8	0	4	1.1	1.2	34
4	0	0	−4	0.5	1.9	155
4	2	0	−3	3.0	1.9	95
4	4	0	−2	3.5	1.2	62
5	4	−4	−2	3.0	2.6	108
5	8	−4	0	0.5	3.8	80
6	0	0	0	5.0	2.6	35
6	4	0	2	1.5	4.3	16
7	0	−2	−6	1.5	1.1	147
7	4	−2	−4	2.0	2.6	97
7	6	−2	−3	1.7	3.1	48
			Dications			
3′	0	0	0	5.0	100	0
3′	2	0	1	0.7	100	115
3′	4	0	2	2.2	22	157

[a] N_H is number of extra H atoms included on Rh_4 cluster core, x and y are the number of $BH_2N(CH_3)_2$ and H_2 molecules required for mass balance, Δt_{eq} is the time spent in equilibration, Δt is equilibrated trajectory length, and $\Delta U_{x,y}$ is relative energy as defined in text. Approximate error on $\Delta U_{x,y}$ is estimated to be ±5 kcal/mol due to finite sampling.

(15) Douglas, T. M.; Chaplin, A. B.; Weller, A. S. *J. Am. Chem. Soc.* **2008**, *130*, 14432.
(16) (a) Car, R.; Parrinello, M. *Phys. Rev. Lett.* **1985**, *55*, 2471–2474. (b) Payne, M. C.; Teter, M. P.; Allen, D. C.; Arias, T. A.; Joannopoilos, J. O. *Rev. Mod. Phys.* **1992**, *64*, 1045. (c) Kuhne, T. D.; Krack, M.; Mohamed, F. R.; Parrinello, M. *Phys. Rev. Lett.* **2007**, *98*, 066401.
(17) Perdew, J. P.; Burke, K.; Ernzerhof, M. *Phys. Rev. Lett.* **1996**, *77*, 3865.
(18) (a) VandeVondele, J.; Krack, M.; Mohamed, F.; Parrinello, M.; Chassaing, T.; Hutter, J. *Comput. Phys. Commun.* **2005**, *167*, 103. (b) Lippert, G.; Hutter, J.; Parrinello, M. *Mol. Phys.* **1997**, *92*, 477.
(19) Henkelman, G.; Uberuaga, B. P.; Jonsson, H. *J. Chem. Phys.* **2000**, *113*, 9901.

due to insufficient sampling of configuration space from the short duration of our simulations. A conservative error bar for $\langle \Delta U \rangle$ of approximately ±5 kcal/mol is estimated by comparing the energies of separate runs, obtained from different starting configurations, for several isomers. This limits our ability to discriminate the relative energies of various isomers to within a window of approximately 10 kcal/mol.

In order to put the average energies on the same relative scale, we consider the quantity

$$\Delta U_{x,y} = \langle U_A \rangle - x\langle U_{BH_2NMe_2} \rangle - y\langle U_{H_2} \rangle$$

where $\langle U_A \rangle$ is the average potential energy of the system, A, that is determined from the constant temperature ensemble average at 300 K, $\Delta U_{x,y}$ is proportional to the average energy difference between products and reactants in the equilibrium represented by:

$$Rh_4(BH_2N(CH_3)_2)_8 + xBH_2N(CH_3)_2 + yH_2 \leftrightarrow Rh_4H_{2y}(BH_2N(CH_3)_2)_{8+x}$$

This grand canonical ensemble approach allows us to compare the *relative* energies of species with differing stoichiometries on the same scale, thus enabling us to use average energy as a criterion, in addition to structural quantities, for choosing the best representation of the catalyst resting state. Data for $\langle U_{x,y} \rangle$ are presented in Table 1.

2.2. Experimental Methods. The Rh_4 cluster sample was prepared in toluene, starting from $[RhCODCl]_2$ (where COD is 1,5-cyclooctadiene) as per previously reported.[13] The solid was isolated from the solvent by filtration after 24 h and was washed thrice with toluene. The solid pressed onto clean double sided Nichiban tape supported by 1 cm × 3 cm flat Si wafer inside a N_2 recirculated glovebox with <1 ppm O_2 and H_2O. The Si wafer piece containing the sample was sealed into clean VWR trace clean sample vials (cat. no. 15900-026) for the short 1 min transfer into the glovebag attached to XPS system. The Si wafer containing the sample was mounted for XPS inside a nitrogen-purged I^2R glovebag attached to the XPS sample introduction chamber. The samples were exposed to the glovebag environment for only about 1 to 2 min during the transfer into the spectrometer. The glovebag is continually purged with nitrogen (<1 ppm oxygen) from LN_2 evaporation. The oxygen concentration in the glovebag during the XPS sample mounting was measured at <30 ppm oxygen. The sample holder was then placed into the XPS vacuum introduction system and pumped to $<1 \times 10^{-6}$ Torr using a turbomolecular pumping system prior to introduction into the main ultrahigh vacuum system. The main vacuum system pressure is maintained at $<5 \times 10^{-9}$ Torr during analysis and pumped using a series of sputter ion pumps.

XPS measurements were performed using a Physical Electronics Quantum 2000 Scanning ESCA Microprobe. This system uses a focused monochromatic Al Kα X-rays (1486.7 eV) source and a spherical section analyzer. The instrument has a 16 element multichannel detector. The X-ray beam used was a 100 W, 100 μm diameter beam that was rastered over a 1.3 mm by 0.2 mm rectangle on the sample. The X-ray beam is incident normal to the sample, and the photoelectron detector was at 45° off-normal. The high energy resolution photoemission spectrum was collected using a pass energy of 46.95. For the $Ag3d_{5/2}$ line, these conditions produced fwhm of better than 0.98 eV. The binding energy (BE) scale is calibrated using the Cu $2p_{3/2}$ feature at 932.62 ± 0.05 eV and Au 4f at 83.96 ± 0.05 eV for known standards. The sample experienced variable degrees of charging. Low energy electrons at ~1 eV, 20 μA, and low energy Ar^+ ions, were used to minimize this charging.

3. Results

3.1. Charge State of Rh_4 Species. The assignment of the overall charge of the Rh_4 cluster intermediates observed under catalytic operando conditions is at best approximate due to limitations in the experimental techniques deployed. Nonetheless we are able to assign an approximate range by considering the results of XAFS, MS, and XPS.

Although the X-ray absorption near-edge spectrum potentially holds information about the metal oxidation state, in the case of rhodium, the core-hole lifetime broadening at 23.2 keV edge limits the energy resolution to greater than about 6 eV. By comparing our previous XAFS results[13] starting from $[RhCODCl]_2$ in either THF or toluene in the presence of dimethylamino borane, with known rhodium compounds, we can only state that the oxidation state of the observed resting state of the catalyst is between Rh(0) and Rh(I), from this data. The XAFS data show that there is no Rh(II) or Rh(III) in the system. This is consistent with the known chemistry of the catalytic system where the starting material, $[Rh(1,5\text{-}COD)Cl]_2$, begins at Rh(I), and since the system is under reducing conditions one can only believe that the oxidation state on the rhodium should decrease to Rh(0) or remain at Rh(I).

To further resolve this issue, electrospray mass spectroscopy was attempted on the reaction mixture in toluene but did not yield any rhodium-containing species in fragmentation patterns. Under the same spectroscopic conditions, other organometallic tetrahedral rhodium clusters of the form $[Cp^*RhH]_4[X]_2$ (X = PF_6, BF_4, and Cl) and their reaction products were observed.[26] We theorized from this that perhaps the rhodium clusters derived from the amine borane reactions were not charged, or alternately were not easily charged, precluding mass spectroscopic observation.

Unfortunately, XPS studies on isolated species are also inconclusive as to the overall charge on the cluster but suggested either a neutral or dicationic species. The XPS results which showed 1 Cl per 2 Rh did suggest that the species formed were charged due to the absence of any direct Rh−Cl interactions in the XAFS spectra.[13] This would lead the Rh_4 clusters to a +2 charge which would be countered by two chloride ions observed by XPS. This again is consistent with the XAFS results that showed that the oxidation state of the rhodium was less than +2.

Overall, our experimental findings suggest that the Rh atoms in the cluster are in an oxidation state of 1 or less, and that the overall cluster intermediate observed in XAFS has a net charge between 0 and +4, which is consistent with known charge states of Rh cluster compounds[20] and can thus serve as a starting point for examining the proposed structures of Scheme 1 using molecular simulation.

3.2. Assignment of Catalyst Resting States via AIMD Simulations. To begin our examination of the proposed catalyst resting, we first note that 300 K AIMD simulations from the various starting configurations of the Rh_4 species depicted in Scheme 1 reveal that for *all* the structures considered there is significant fluxional behavior, including large amplitude motions, that leads to structural rearrangements. This observation adds a degree of complexity to the search for a cluster species that are consistent with XAFS. The previous fits to experimental data assumed a single well-defined structure as opposed to an ensemble of isomers in thermal equilibrium. To include this added feature in our analysis, we first illustrate the types of dynamical motion the proposed structures can undergo. Then we extract likely candidates for the catalyst resting state based on relative isomer energetics and geometrical constraints.

(20) Weller, A. S.; McIndoe, J. S. *Eur. J. Inorg. Chem.* **2007**, 4411.

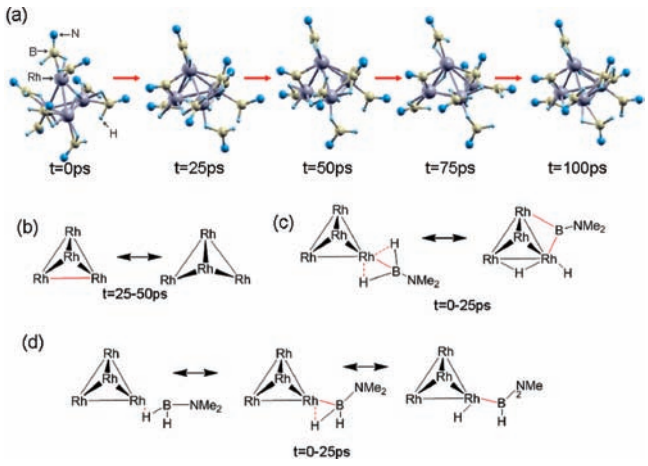

Figure 1. (a) Structure of $Rh_4(BH_2NMe_2)_8^{2+}$ (**3′**H_0^{2+}) at 300 K are shown at 25 ps intervals. Methyl groups have been subtracted for clarity. Atom colors: N, blue; B, yellow; H, light blue; Rh, gray. Bonds are drawn between atoms which have an interaction distance compatible with the sum of their covalent radii and are not indicative of a detailed bonding analysis based on the underlying electronic structure. Key fluxional processes seen in the AIMD trajectory are illustrated schematically: (b) Rh_4 cluster isomerization, (c) terminal to bridge ligand migration, (d) terminal ligand binding isomerization and hydride transfer. The times indicated in parentheses in b−d are indicative of where this process may be seen in the configurations given in the MD configurations presented in a.

The types of motions typically observed in our AIMD simulations can be best understood with the illustrated example of $Rh_4(BH_2NMe_2)_8^{2+}$ (Me = CH_3) with no additional hydrogen (which is derived from dication of structure **3′** with no additional H atoms and denoted as **3′**H_0^{2+}) shown in Figure 1a. For this (and all other) species, the potential energy, U, fluctuates by about 10 kcal/mol at 300 K, which makes processes with energy barriers of that magnitude, or less, relatively facile. Thus, several dynamical processes are observed during the course of the 100 ps of an equilibrated trajectory:

(i) The Rh_4 cluster isomerizes between a pure tetrahedral species and a more open species where a single Rh−Rh bond elongates, illustrated schematically in Figure 1b. This occurs between 25 and 50 ps, and the reverse process of re-forming the tetrahedron occurs between 75 and 100 ps. Although tetrahedral clusters are local minima for most neutral and dicationic isomers considered, all simulations show significant isomerization of the Rh cluster core and only a few have a high percentage of tetrahedral configurations.

(ii) Terminal BH_2NMe_2 ligands migrate to bridging configurations (see Figure 1c) as found in structure **5**, as seen for example between 0 and 25 ps, and later between 75 and 100 ps with a single transient Rh−N bond as in structure **6**.

(iii) These same terminal ligands fluctuate between a species with a close Rh−B contact (ca. 2.1−2.2 Å) and one where Rh and B are separated by about 2.5−2.6 Å and bridged by a hydride, illustrated in Figure 1d. The binding geometries are in good accord with known mononuclear crystal structures: the former with the observed mononuclear Rh species of ref 15 whereas the latter is in accord with B−H/M σ complexes observed in ref 25. The interconversion between these configurations is also observed to be reversible as can be seen by following the lowest terminal ligand in Figure 1a which undergoes this transition between 0 and 25 ps and the reverse process between 75 and 100 ps.

(iv) Reversible exchange of B−H hydrides with the Rh_4 cluster (see Figure 1d) leaving $BHNMe_2$ ligands similar to structure **7**; for an example, compare the furthest right terminal ligand between 0 and 25 ps. This observation indicated that hydride can readily migrate from B to Rh with negligible energy cost, which is in accord with the inability to observe these species in NMR.[13]

(v) Though not seen for **3′**H_0^{2+}, ligand dissociation with little potential energy cost at 300 K is observed for neutral species based on structures **2** and **3′**, indicating that this process is energetically facile at room temperature.

All other MD trajectories exhibit many of these processes as well as other processes such as H insertion into Rh−Rh bonds. The observed fluxionality indicates that many of the proposed structural features in Scheme 1 are not independent well-defined isomers but are in a rapid thermal equilibrium and that a single well-defined structure is not appropriate for describing either the relative energetics or spectroscopic properties.

Given the pronounced fluxional behavior, each configuration in Scheme 1 may be viewed as a starting configuration from which our short time MD simulation may be used to evaluate the relative energetics of all nearby configurations. For an energy comparison of the structural candidates, we thus consider the average potential energy (DFT total energy) $\langle U \rangle$ at 300 K of the equilibrated configurations from our MD trajectory. In the context of the observed fluxional behavior, $\langle U \rangle$ represents the Boltzman weighted potential energy (including vibrational energy) of the structural candidate and any other local minima which may be readily accessed. We then mass balance this quantity by including the average energies for BH_2NMe_2 and H_2 molecules in a grand canonical approach (described above) to account for the differing stoichiometries; see Table 1.

The lowest energy neutral configuration is generated by starting from structure **3′** where two additional H atoms have been added to the Rh_4 cluster core (denoted **3′**H_2). Isomers of structures **1** and **2** are found to be >50 kcal/mol higher in energy, indicating that species where the BH_2NMe_2 ligands are dimerized, prior to dissociation from the cluster, and are energetically disfavored. Structure **3** and **4** with $NHMe_2$ groups are found to be higher in energy by over 50 kcal/mol, which indicates the energetic preference for nonprotonated amines. Structures **5** and **7** are unfavorable by similar amounts when only a few extra H atoms are included on the Rh_4 cluster but in general lower their energy as more hydrogen is added. These extra H atoms however are found to migrate out to the ligands during the MD simulation creating bonding motifs similar to those observed in structure **3′**. Structure **6**, which has the same stoichiometry as **3′**, is not stable, and almost all the Rh−N contacts break in the course of a short-term MD run and convert into configurations similar to that of **3′**, indicating that the direct Rh−N bonding is not favorable. The **3′** family of structures produces the lowest $\langle U \rangle$ values and also shows interesting dynamical behavior including ligand dissociation as well as Rh_4 cluster isomerization.

These observations suggest that both protonated and dimerized ligands may be discounted in our search because of their relatively high energetics. Furthermore, the number of hydrides present in the system either on the boron or the Rh cluster is critical for maintaining the integrity of the Rh_4 cluster core. An insufficient hydride concentration to saturate the boron atoms with approximately two hydrides is unfavorable, and results in products where the central Rh_4 tetrahedron is disrupted by insertion of B into the cluster framework as observed in AIMD trajectories with structures **5** and **7** with no additional H. On the other hand, larger amounts of excess hydride residing on

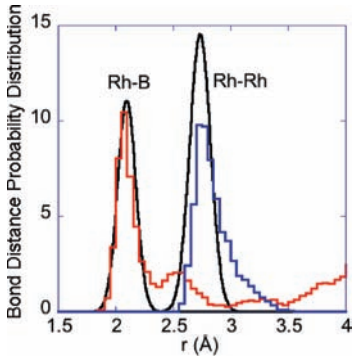

Figure 2. Distribution of Rh−B (red) and Rh−Rh (blue) bond lengths from 300 K AIMD simulation of $\mathbf{3'}H_0^{2+}$ structure. The average Rh−Rh and Rh−B bond length extracted from our previous fits to XAFS data and broadened by the estimated 0.0082 and 0.0063 Å^2 Debye−Waller factors for Rh−Rh and Rh−B distances, respectively, are shown in black for comparison.

the Rh atoms also disrupt the framework leading to hydride intercalation into the Rh−Rh bonds as most notable for the higher hydride counts of structure **3′**. Most significantly, however, in all the MD scenarios considered, the neutral Rh_4 cluster does not remain tetrahedral but rather opens up through the loss of one or more Rh−Rh bonds. Hence, it seems unlikely that a neutral rhodium species can account for the observed XAFS signal.

Given the uncertainty of charge on the tetrahedral rhodium cluster, we also have considered Rh_4^{2+} species (also supported by XPS studies of recovered catalyst solid). For these clusters, we focused our attention on the family of isomers generated from structure **3′** and performed longer trajectories, 20−100 ps, in order to allow the system the maximum opportunity to isomerize. The lowest energy configuration was found for the structure with no additional hydrogens added to the Rh_4 cluster (denoted $\mathbf{3'}H_0^{2+}$) with an increase of 115 and 157 kcal/mol when two and four H are added. Furthermore, the simulations for $\mathbf{3'}H_2^{2+}$ and $\mathbf{3'}H_4^{2+}$ lead to isomerization of the Rh_4 cluster away from a tetrahedral geometry whereas there are only transient fluctuations (see Figure 1) for $\mathbf{3'}H_0^{2+}$. A further comparison of the Rh−B and Rh−Rh bond distance distributions compiled over the MD trajectory (see Figure 2) are also in good agreement with the quantities extracted from our previous fit to the experimental XAFS data.[5] For instance Rh−B and Rh−Rh bond length distributions, with maxima at 2.1 and 2.7 Å, respectively, are in excellent accord with our previous average bond lengths as extracted from FEFF8 fits. However, the Rh−Rh bond length distribution, while unimodal, is significantly broader than that which one would obtain using the Debye−Waller factor ($\sigma^2 = 0.0082$ Å^2) from our previous fit. The Rh−B distance distribution is even more significantly broadened and multimodal, resulting from the multiple ligand binding configurations observed in the MD, with a second maxima at 2.5 Å resulting form the Rh-BH_2NMe_2 σ-complex and a broad continuum at larger distances from nonbonded Rh ligand separations. A detailed re-examination of the XAFS data based on this dynamical picture of the cluster will be considered in detail in the next subsection.

For completeness we also examined a few isomers of the Rh_4^{4+} cluster, where the Rh atoms would each have a formal Rh(I) oxidation state. Our most extensive search was for the structure $\mathbf{3'}H_4^{4+}$ which isomerized away from a tetrahedral geometry within a 6 ps AIMD trajectory at 300 K. Other isomers $\mathbf{2}H_0^{4+}$, $\mathbf{5}H_8^{4+}$, and $\mathbf{7}H_6^{4+}$ are all over 30 kcal/mol higher in energy than the **3′** isomer and isomerizes to species where the four Rh atoms form a butterfly configuration during the local geometry optimization, indicating that a tetrahedral species is not even a stable local minimum on the potential energy surface. Though by no means a definitive search, this data strongly suggests that the more highly charged clusters are less likely to form Rh_4 tetrahedra and agrees both with our above experimental analysis and the net charge on known Rh_4 cluster species from the literature.[20]

To summarize the results of our extensive structural search, the following were found: (i) All the species studied undergo large thermal fluctuations and isomerization at room temperature. (ii) The low energy neutral structures (within 20 kcal/mol of the lowest energy structure) do not exhibit a significant population of Rh_4 tetrahedra and are thus unlikely able to account for the observed XAFS signal. (iii) Highly positively charged +4 cations also isomerize away from tetrahedral species and thus are not likely candidates. (iv) The dications show large percentages of Rh_4 tetrahedra in their AIMD trajectories, the lowest energy belonging to $\mathbf{3'}H_0^{2+}$. Thus, our extensive structural search suggests that the most likely candidate for the catalytic resting state is $\mathbf{3'}H_0^{2+}$ with the caveat that structural features from models **5**, **6**, and **7** are also present in a dynamical equilibrium.

3.3. Comparison with Experimental XAFS. To further test the hypothesis that the $\mathbf{3'}H_0^{2+}$ structure represents the catalytic resting state of the Rh_4 cluster, we compare our simulation results with the previously reported XAFS measurements via the MD-XAFS procedure.[21,22] In this procedure an MD configuration is sampled periodically and a structure extracted for which an XAFS spectrum is calculated. By ensemble averaging the calculated spectra for individual species we are able to model a total XAFS spectrum that includes anharmonic nuclear motion such as that found in our Rh_4 cluster isomers.

As input for the MD-XAFS procedure, an ensemble of clusters was generated by sampling the 100 ps equilibrated MD trajectory every 50 fs. For each configuration, each of the four Rh atoms in the cluster were separately chosen to be the photoelectron source and used as input into the FEFF8 electron multiple scattering code[14,23] where the EXAFS fine structure, $\chi(k)$ was generated. In Figure 3a, the ensemble averaged fine structure, $\bar{\chi}(k)$, was then accumulated and compared to experimental measurement. The model successfully reproduces the complicated series of oscillations in $k^2\chi(k)$ observed in the experimental spectrum with no additional peaks. Moreover, other trajectories such as $\mathbf{3'}H_2$, $\mathbf{3'}H_4$, and $\mathbf{3'}H_2^{2+}$, which were also tested by this procedure, do not even qualitatively account for the oscillations in $k^2\chi(k)$ as a result of the large percentage on nontetrahedral Rh_4 clusters observed in those trajectories. This latter observation underscores the sensitivity of the XAFS measurement with respect to the underlying structure and points to the fact that the ensemble generated from $3'H_0^{2+}$ is a unique match to the experimental spectrum.

The magnitude of the oscillations at $k > 9$ Å^{-1} are perfectly reproduced; however, there is a notable discrepancy for lower k values. To understand the source of this, we obtain a real

(21) Palmer, B. J.; Pfund, D. M.; Fulton, J. L. *J. Phys. Chem.* **1996**, *100*, 13393.
(22) Dang, L. X.; Schenter, G. K.; Glezakou, V. A.; Fulton, J. L. *J. Phys. Chem. B* **2006**, *110*, 23644.
(23) Zabinsky, S. I.; Rehr, J. J.; Ankudinov, A.; Albers, R. C.; Eller, M. J. *Phys. Rev. B* **1995**, *52*, 2995.

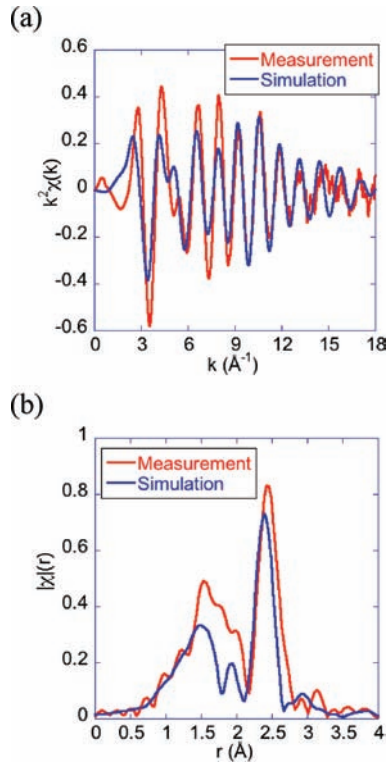

Figure 3. MD-EXAFS results for $\mathbf{3'}H_0^{2+}$. (a) Average $k^2\chi(k)$. (b) Real space pair distribution, $|\chi|(r)$.

space representation of the XAFS spectra, $|\chi|(r)$, by calculating the discrete Fourier transform of the structure factor as implemented in the FEFFIT package[24] using a Hanning window function; see Figure 3b. The function $|\chi|(r)$ from the experimental data is characterized by two broad peaks at about 1.5 and 2.5 Å corresponding to nearest neighbor Rh−B and Rh−Rh distances, respectively. Note that these peaks do not correspond to the real space bond distances, as represented in Figure 2, because of the inherent phase shift of the photoelectron scattering in the XAFS process. Our model successfully accounts for the latter of the two peaks; however, the amplitude in the range from 1.5−2.0 Å is not quantitatively reproduced which thus implies an underestimation in the scattering amplitude of Rh−B contacts. The differences in the $\chi(k)$ magnitudes at low k and the Rh−B amplitudes in $|\chi|(r)$ can be ascribed to differences in the estimated the absorption edge energy, E_0, and the bond lengths (for Rh−Rh) between the simulated and the experimental spectra. The combination of E_0 shift with small differences in the bond lengths (for Rh−Rh) causes some *destructive interference* from Rh−B and Rh−Rh scattering oscillations at low k.

The effect of the adsorption edge and bond length parameters are properly accounted for by fitting the experimental or simulated data to the theoretical standards generated from the FEFF8 scattering code. This procedure was used to generate the experimental Rh−B and Rh−Rh pair distribution functions given in Figure 2. As noted in Section 3.2, the primary peak for the experimentally determined Rh−B interaction is in excellent agreement with the simulated structure both in terms of the Rh−B bond distance and B coordination number (from the integrated area). From the model structure, there is a small secondary Rh−B peak at 2.5−2.6 Å, arising from the σ-complex ligand binding configuration, that is not detected in the experimental spectra. For a light element such as B, the longer distance and the higher disorder of this peak would put this feature at the limits of detection for the XAFS process. Thus, it can be concluded that the variations between the experimentally and theoretical Rh−B bond length distributions are within the ability of XAFS to properly distinguish.

Since the frequency of the XAFS oscillations, as a function of k, are well reproduced as well as their damping a high k values, it can be safely assumed that our AIMD ensemble contains accurate representations of the structures as well as the magnitude of their structural fluctuations. However, the relative populations of the various ligand binding configurations and the correlations between them (the ligand disorder) are not expected to be quantitatively accounted for in our simulation, as the observed motions are slow on the picosecond time scale, and hence, even with our relatively long AIMD simulation, it is unlikely that these motions have been sufficiently sampled. Furthermore, although solvent effects on the XAFS signal have been reported to be negligible,[13] our AIMD simulation is performed in gas phase whereas the experimental spectrum is performed in THF (and toluene) solution, and thus, even in the limit of ergodic sampling, we could not expect perfect agreement in the bond distance distributions between theory and experiment because of possible influences on the populations of the various ligand binding configurations. Nonetheless, the overall agreement in the main features of the XAFS spectrum is striking and further strengthens our conviction that our dynamic model of the $\mathbf{3'}H_0^{2+}$ species is a unique solution for the catalyst resting state.

In passing it is noted that our previous assignment of the XAFS spectra included an admixture of both Rh_4 and Rh_6 clusters in a 4:1 ratio.[13] This assignment was based largely on the presence of 5% probability of long Rh−Rh contacts on the order of 3.0 Å. Our current simulation which contains approximately 25% of the Rh_4 species in an open configuration (see Figure 1b) can account for this observation (1/6 bonds, 25% of the time is 4% probability) without invoking the presence of larger Rh clusters. Though we cannot definitively rule out the presence of these larger Rh clusters, our simulations are suggestive that nontetrahedral Rh_4 clusters *may* be a cause of this feature in the experimental spectrum.

3.4. Reaction Pathways. Starting from this known structure of the catalyst resting state, $Rh_4(BH_2NMe_2)_8^{2+}$, we use insight gained from AIMD results and additional CI-NEB calculations of minimum energy reaction paths to develop a proposed mechanism for the dehydrogenation process, as shown in Figure 4. Our mechanism involves the following fundamental steps, the first four involving the tetrahedral rhodium cluster and the last the thermal dimerization of the departing ligand leading to the products observed by ^{11}B NMR:

$$[Rh_4(BH_2NMe_2)_8]^{2+} \rightarrow [Rh_4(BH_2NMe_2)_7]^{2+} + BH_2NMe_2 \quad (1)$$

(24) Newville, M.; Ravel, B.; Haskel, D.; Rehr, J. J.; Stern, E. A.; Yacoby, Y. *Physica B* **1995**, *209*, 154.
(25) Kawano, Y.; Yamaguchi, K.; Miyake, S.; Kakizawa, T.; Shimoi, M. *Chem.—Eur. J.* **2007**, *13*, 6520.
(26) Linehan, J.; Finke, R., unpublished data.

$$[Rh_4(BH_2NMe_2)_7]^{2+} + BH_3NMe_2H \rightarrow [Rh_4(BH_2NMe_2)_7BH_3NMe_2H]^{2+} \quad (2)$$

$$[Rh_4(BH_2NMe_2)_7BH_3NMe_2H]^{2+} \rightarrow [Rh_4H(BH_2NMe_2)_7(BH_3NMe_2)]^{2+} \quad (3)$$

$$[Rh_4H(BH_2NMe_2)_7(BH_3NMe_2)]^{2+} \rightarrow [Rh_4(BH_2NMe_2)_8]^{2+} + H_2 \quad (4)$$

$$2BH_2NMe_2 \rightarrow (BH_2NMe_2)_2 \quad (5)$$

To obtain an energy estimate for this process, we report $T = 0$ K electronic energies and do not attempt, at this stage, to estimate either a vibrational component to the energy or entropy estimates to obtain a free energy for this process because of the extreme challenge of calculating these quantities for what our AIMD results demonstrate to be a strongly *anharmonic* systems. Moreover, this larger number of almost isoenergetic minima suggests that there also exists an ensemble of low energy reaction paths which should have significant effect upon the free energy which are not accounted for in the current analysis. We cannot be certain that the energy paths we have calculated are the lowest ones but rather represent upper bounds. Thus, the reaction energetics reported here are only semiquantiative and are intended to provide energy estimates for these processes.

The reaction steps 1−4 are shown on a relative energy landscape in Figure 4. During the AIMD simulations it was noted that dissociation of a BH_2NMe_2 ligand, reaction 1, is facile at room temperature with an estimated energy for this process of 14 kcal/mol. Two dissociated BH_2NMe_2 molecules can then form $(BH_2NMe_2)_2$ in solution with a net energy release of 15 kcal/mol; reaction 5 is also in accord with previous findings.[12a] Note that from our results in Section 3.2, dimerization prior to dissociation was found to be unfavorable and our mechanism is consistent with BH_2NMe_2 intermediates observed in time-resolved ^{11}B NMR experiments.[7b]

The ligand dissociation creates a vacant site on the Rh_4 cluster creating the species $[Rh_4(BH_2NMe_2)_7]^{2+}$ which is the active catalyst in our dehydrogenation cycle. A BH_3NMe_2H species can coordinate to this catalyst at the vacant coordination site, reaction 2, which is a net 27 kcal/mol exothermic process. The next two reaction steps form the largest potential barriers in the cycle. The first is N−H to Rh hydrogen transfer, reaction 3, followed by release of H_2, reaction 4, which have barriers 24 and 12 kcal/mol, respectively. Given that the product of reaction 3 leads to a trapped intermediate which may revert to the protonated amino group more readily than release hydrogen via reaction 4, the kinetic barrier for dehydrogenation would thus arise from a combination of the two reactions and would involve a net 28 kcal/mol barrier. On the basis of our observations from AIMD at 300 K, boron to rhodium hydride transfer is rapid and thus has negligible energy barriers, and as a result, hydride transfer from the BH_3 group onto the Rh_4 cluster creating a BH_2NMe_2 ligand and regenerating the catalyst is facile. The estimated overall activation energy for the proposed catalytic cycle is significantly less than the 45 kcal/mol obtained for the uncatalyzed dehydrogenation process and should be feasible at room temperature.

The proposed mechanism bears strong resemblance to those proposed for dehydrogenation of amino boranes by mononuclear Ni[7e,11a] complexes in that the reported catalytic cycles show that nitrogen deprotonation and H_2 release possess the largest barriers, which are on the order of those reported here whereas hydride transfer from boron is found to be facile. Unlike the Ir pincer catalyst of ref 11b, we do not find a concerted H_2 release mechanism which for the current system has an energy barrier on the order of the uncatalyzed reaction. Finally, the energy landscape of this process is strikingly similar for other likely resting state candidates such as $Rh_4H_2(BH_2NMe_2)_8$ where reaction energies and computed barriers varied only at most by 5 kcal/mol, indicating that the mechanism is relatively insensitive to the fine details of the catalyst structure.

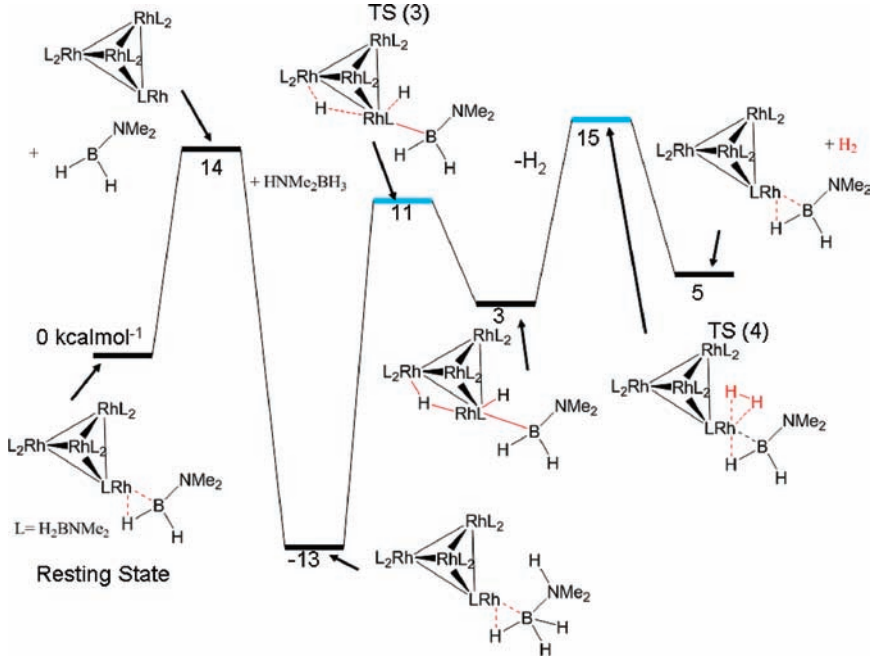

Figure 4. Calculated energy differences between Rh_4 cluster intermediates and transition states leading to dehydrogenation of dimethylaminoborane by $\mathbf{3'}H_0^{2+}$. Black (Blue) lines represent relative energies of intermediates (transition states). Insets show schematic structure of relevant intermediates and transition states; TS (3) and TS (4) refer to the transition states of reactions 3 and 4 of the text respectively. All energies are quoted in kcal/mol.

4. Conclusions

In summary, by the use of AIMD and MD-XAFS, we have identified the structure of the resting state of the Rh_4 cluster-based homogeneous catalyst for the dehydrogenation of aminoboranes. Our theoretical structures match well with single crystal studies of metal aminoborane complexes reported in the literature,[15,25] but we find that the proposed Rh_4 species are highly fluxional. From this proposed resting state, we have inferred a reaction mechanism for the extraction of H_2 from BH_3NMe_2H which we estimate reduces the hydrogen release barrier significantly relative to that for the isolated molecule. Our proposed mechanism suggests that N−H to metal proton transfer and H_2 release are the key rate-determining steps in the dehydrogenation process. This in turn suggests that catalyst modification of the metal proton/hydride affinities is the most promising route for designing effective catalysts for this process. Future work will focus on further probing this mechanism by time-resolved NMR spectroscopic measurements and free energy-based MD methods for obtaining reaction free energies as well as investigating other catalysts based on other transition metals.

In general, our ability to effectively use state-of the-art simulation techniques in conjunction with sophisticated operando catalysis measurements strengthens our conviction that the ambitious combination of theory and experiment deployed in a complementary fashion can lead to unprecedented levels of understanding on systems of very high chemical complexity.

Acknowledgment. This work was supported by the U.S. Department of Energy Office of Basic Energy Sciences, Chemical Sciences Division. Pacific Northwest National Laboratory (PNNL) is operated for the U.S. DOE by Battelle under contract no. DE-AC06-76RLO 1830. Computational resources were provided by the National Energy Research Scientific Computing Center at Lawrence Berkeley National Laboratory. XPS studies were performed using EMSL, a national scientific user facility sponsored by the Department of Energy's Office of Biological and Environmental Research located at PNNL. PNC/XOR facilities at the Advanced Photon Source, and research at these facilities, are supported by the US Department of Energy - Basic Energy Sciences, a major facilities access grant from NSERC, the University of Washington, Simon Fraser University, the Pacific Northwest National Laboratory, and the Advanced Photon Source. Use of the Advanced Photon Source is also supported by the U.S. Department of Energy, Office of Science, Office of Basic Energy Sciences, under contract no. DE-AC02-06CH11357.

Supporting Information Available: Structures and absolute energies (atomic units) of all minima and transition states calculated for the dehydrogenation mechanism in Scetion 3.4. This information is available free of charge via the Internet at http://pubs.acs.org/.

JA901480U